Wang *et al.*
Cell Communication and Signaling (2024) 22:594
https://doi.org/10.1186/s12964-024-01978-z

Cell Communication and Signaling

RESEARCH

Open Access

Adipose tissue protects against skin photodamage through CD151- and AdipoQ-EVs

Yan-Wen Wang[1,2†], Poh-Ching Tan[1†], Qing-Feng Li[1*], Xue-Wen Xu[2*] and Shuang-Bai Zhou[1*]

Abstract

To clarify the protective effects of subcutaneous adipose tissue (SAT) against photodamage, we utilized nude mouse skin with or without SAT. Skin and fibroblasts were treated with adipose tissue-derived extracellular vesicles (AT-EVs) or extracellular vesicles derived from adipose-derived stem cells (ADSC-EVs) to demonstrate that SAT protects the overlying skin from photodamage primarily through AT-EVs. Surprisingly, AT-EVs stimulated fibroblast proliferation more rapidly than ADSC-EVs did. The yield of AT-EVs from the same volume of AT was 200 times greater than that of ADSC-EVs. To compare the differences between AT-EVs and ADSC-EVs, we used a proximity barcoding assay (PBA) to analyze the surface proteins on individual particles of these two types of EVs. PBA analysis revealed that AT-EVs contain diverse subpopulations, with 83.42% expressing CD151, compared to only 1.98% of ADSC-EVs. Furthermore, AT-EVs are internalized more rapidly by cells than ADSC-EVs, as our study demonstrated that CD151-positive AT-EVs were endocytosed more quickly than their CD151-negative counterparts. Additionally, adiponectin in AT-EVs activated the AMPK pathway and inhibited the NF-κB pathway, enhancing fibroblast protection against photodamage. The significantly higher yield and faster acquisition of AT-EVs compared to ADSC-EVs underscore their potential for broader applications.

Keywords Adipose tissue, Adipose tissue-derived extracellular vesicles, UVB, Skin photoaging, CD151, Endocytosis

Graphical Abstract

AT mitigates skin photoaging via AT-EVs, which consist of 14 subpopulations and express more CD151 and APN on their surface, as determined by PBA sequencing. CD151 facilitates faster cellular recognition and uptake of AT-EVs. APN activates AdipoR to stimulate the AMPK pathway and inhibit the NF-κB pathway, reducing ROS and DNA damage

†Yan-Wen Wang and Poh-Ching Tan have contributed equally to this work.

*Correspondence:
Qing-Feng Li
dr.liqingfeng@shsmu.edu.cn
Xue-Wen Xu
xxw_0826@163.com
Shuang-Bai Zhou
shuangbaizhou@yahoo.com
Full list of author information is available at the end of the article

© The Author(s) 2024. **Open Access** This article is licensed under a Creative Commons Attribution-NonCommercial-NoDerivatives 4.0 International License, which permits any non-commercial use, sharing, distribution and reproduction in any medium or format, as long as you give appropriate credit to the original author(s) and the source, provide a link to the Creative Commons licence, and indicate if you modified the licensed material. You do not have permission under this licence to share adapted material derived from this article or parts of it. The images or other third party material in this article are included in the article's Creative Commons licence, unless indicated otherwise in a credit line to the material. If material is not included in the article's Creative Commons licence and your intended use is not permitted by statutory regulation or exceeds the permitted use, you will need to obtain permission directly from the copyright holder. To view a copy of this licence, visit http://creativecommons.org/licenses/by-nc-nd/4.0/.

in fibroblasts. This results in improved skin histology, increased collagen production, a reduction in senescent cells, and decreased ROS accumulation. (Created with BioRender.com)

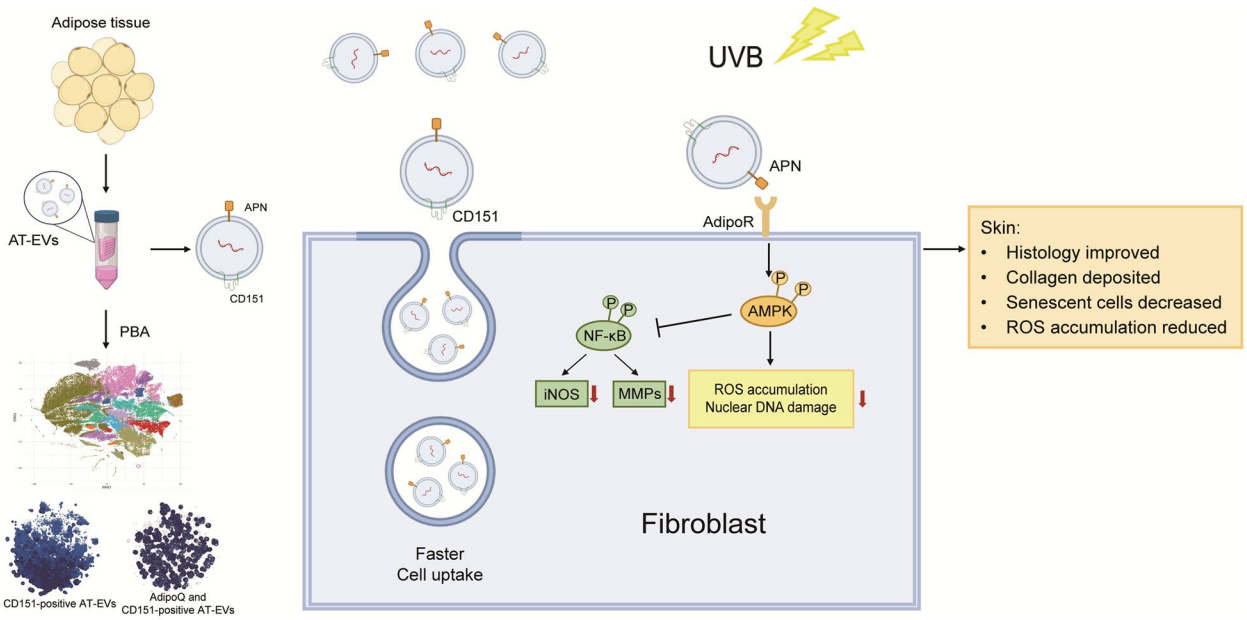

Introduction

Photodamage is the most common and primary extrinsic cause of skin ageing [1]. This type of damage not only leads to a rough texture and wrinkled appearance but can also cause skin immune dysfunction and impaired skin barrier function, leading to dermatitis, melanin spots, poor wound healing, and even malignant skin tumours [2–5]. Ultraviolet B (UVB) light is recognized as a harmful component of sunlight and can easily lead to skin photoaging during sun exposure [6]. UVB radiation promotes the generation and accumulation of reactive oxygen species (ROS) and induces DNA damage [7–9]. Subcutaneous adipose tissue (SAT) is closely associated with the skin. Clinical observations have shown that areas rich in SAT tend to have better skin texture than areas without SAT [10–12]. Fat transplantation can soften scars, ameliorate skin discolorations, smooth wrinkles, improve skin texture, and promote hair follicle regeneration [13, 14]. However, whether adipose tissue (AT) has a protective effect on the skin and the underlying mechanisms are unclear.

AT is primarily composed of lipid-rich cells known as adipocytes, along with stromal vascular fraction cells (SVFs) that consist of adipose-derived stem cells (ADSCs), preadipocytes, endothelial cells, and immune cells. Cells derived from AT, such as ADSCs or vascular endothelial cells [15, 16], can migrate to adjacent tissues and differentiate into somatic cells during skin expansion or wound healing [17]. However, the limited number of migrating cells has minimal impact. Extracellular vesicles (EVs) are cell-secreted membranous vesicles that deliver RNAs, proteins, and lipids to recipient cells, serve as mediators of intertissue communication and exert regulatory effects [18]. Adipose tissue-derived extracellular vesicles (AT-EVs) are a mixture of EVs produced by various AT cells [19]. The composition of AT-EVs includes EVs derived from adipose-derived stem cells (ADSC-EVs), but AT-EVs are more diverse than ADSC-EVs. Notably, ADSCs, through ADSC-EVs, are effective treatments for skin ageing [20] and wound healing [21] and can promote skin regeneration [22]. AT-EVs can promote skin regeneration, which can accelerate diabetic wound healing, as well as cell proliferation and migration [23]. However, whether the protective effect of AT in the skin is mediated by AT-EVs and the underlying mechanisms are worth exploring.

To investigate the role of AT during UVB exposure, we employed a novel inguinal skin model with and without SAT, as well as a fat graft model, to demonstrate the protective effect of AT. After in vivo and in vitro experiments, the effective substances in AT were confirmed to be AT-EVs. Compared with ADSC-EVs, AT-EVs can promote cell proliferation more rapidly, suggesting that AT-EVs are internalized more quickly, which is associated

with EV surface proteins. To compare the surface protein expression of AT-EVs and ADSC-EVs, we used a proximity barcoding assay (PBA) and identified two proteins with relatively high expression rates on AT-EVs. Subsequent in vitro experiments explored the role of these proteins in facilitating the cellular uptake of AT-EVs and their mechanisms of protection against photoaging.

Methods

Treatment with AT and cell culture

Human ATs were acquired from healthy and young female donors with a BMI higher than 18.5 and less than 20 who underwent abdominal liposuction. Each participant provided written consent, and the research protocol received approval from the Ethics Committee of Shanghai Jiao Tong University School of Medicine. The AT was cleaned as previously described [23]. The microfat graft was prepared according to a previously reported procedure [24].

Human ADSCs were isolated from fat mass as described previously [25]. ADSCs were cultured in low-glucose Dulbecco's modified Eagle's medium (DMEM, Gibco, Grand Island, NY, USA) supplemented with 10% foetal bovine serum (FBS, Cyagen, Santa Clara, CA, USA) and 1% antibiotic–antimycotic mixture (Gibco, Grand Island, NY, USA). ADSCs were passaged every 3–7 days, and passage 3 ADSCs were used to prepare ADSC-EVs. Characterization of ADSCs at passage 3 was performed by inducing adipogenic and osteogenic differentiation. Human fibroblasts (HFs) were isolated from the skin dermis as previously described [26]. The NIH3T3 cell line was procured from the Cell Bank of the Chinese Academy of Science (Shanghai, China). Fibroblasts were cultured in high-glucose DMEM (Gibco) supplemented with 10% FBS and 1% antibiotic–antimycotic mixture and passaged every 3–4 days. HFs from passages 2–3 were utilized in the experiments. All the cells were cultured at 37 °C and 5% CO_2. To prevent mycoplasma contamination, DAPI staining was conducted at each cell passage to ensure cell health. Media from NIH3T3 cells was harvested after 24 h of culture in serum-free DMEM when the cells reached 60–70% confluence. Informed consent was secured from all participating patients. The study protocol was reviewed and approved by the Ethics Committee of Shanghai Ninth People's Hospital.

Model of photoaging induced by UVB and its treatment

The in vivo experiments were performed on female BALB/c nude mice. All the mouse experiments were approved by Shanghai Ninth People's Hospital. Fat grafting, UVB irradiation, and gross evaluation were all completed after isoflurane anaesthesia. UVB irradiation was carried out as detailed in a previous publication [20]. The three types of animal experiments were the inguinal skin with and without SAT, the dorsal skin model with and without fat grafts, and the dorsal skin model with ADSC-EVs and AT-EVs.

NIH3T3 cells or HFs were cultured in culture medium or culture medium supplemented with different EVs. After 24 h and two washes with PBS, the cells were exposed to UVB irradiation at a cumulative dosage of 100 mJ/cm^2 following a previous protocol [20]. Then, the culture medium of the cells was replenished with fresh culture medium or culture medium supplemented with different EVs for 24 to 72 h before the experiments were performed.

EV preparation, fluorescent labelling, and cellular uptake of EVs were described minutely in supplementary methods (Supplementary Material 1). The details of the animal or cell group division, gross skin evaluation, tissue histological analysis, assessment of cellular proliferation, cell SA-β-gal staining, immunofluorescence staining, ROS detection, quantitative real-time polymerase chain reaction (qRT–PCR), and western blotting (WB) are listed in the supplementary information.

To verify how AT-EVs exert their effects, NIH3T3 cells with low expression of AdipoR were constructed using the lentivirus, with details provided in the supplementary information.

PBA and EV proteomic data analysis

To determine the surface proteins of EVs from ADSCs and ATs, we employed PBA to identify the presence of 261 proteins on these EVs, as listed in Supplementary Material 2. The process utilized antibodies equipped with DNA probes that bear a distinct protein tag for each protein type [27]. The specific reagents, instruments, and operations used are listed in the supplementary information.

Sequencing reads were obtained via EVisualizer® software (version 1.0; Secretech, Shenzhen, China). Data normality was initially assessed via the Shapiro–Wilk test, and data homogeneity was evaluated via either the F test or Bartlett's test. The Benjamini–Hochberg procedure was applied for p value adjustment. The unsupervised FlowSOM algorithm was employed for the generation of EV subpopulations [28]. Visualization of these subpopulations was achieved via distributed stochastic neighbourhood embedding (t-SNE) and uniform flow approximation and projection methods [29]. Some details of the statistical analysis are listed in the supplementary information.

Isolation of CD151-positive AT-EVs

Superparamagnetic Dynabeads™ were conjugated with a CD151 antibody (BioLegend, San Diego, CA, USA) via a

Dynabeads Antibody coupling kit (Invitrogen, Carlsbad, CA, USA) following the manufacturer's instructions and a previous publication [30]. The details of isolation are described in the supplementary information.

Statistical analysis

Numerical data are presented as the means ± standard deviations. The data were analysed via Student's t test or one-way analysis of variance (ANOVA) followed by Tukey's post hoc test (GraphPad Prism 9.3.1, La Jolla, CA, USA). Confidence intervals were determined at the 95% confidence level, and $P < 0.05$ was considered to indicate statistical significance.

Results

AT has a protective effect on the skin against UVB irradiation

To investigate whether AT protects skin against photoaging, we established two AT models. One model utilized inguinal skin with SAT as the AT group, whereas the adjacent skin without SAT served as the control (Fig. 1a). Before UVB irradiation, HE and Masson staining revealed no significant differences in epidermal or dermal thickness between the two groups (Figs. S1, S2). After 8 weeks of UVB exposure, the AT group presented improved skin elasticity (Fig. 1b). The manifestations of photoaging observed in the skin of nude mice can serve as a model for the pathological changes observed in human ageing skin, with a substantially growing epidermis, thinning dermis, and more aged cells [31]. Histological analyses, including HE, Masson, Sirius Red, and SA-β-gal staining, revealed that the AT group had a thinner epidermis, a thicker dermis, increased collagen content, and fewer senescent cells. These findings indicate that AT strongly contributes to a more youthful appearance of the skin from photoaging (Figs. 1c, S3).

In the alternative model, a fat graft placed beneath the dorsal skin constituted the fat graft group, with PBS injection serving as the control. Two weeks post-transplantation, Oil Red O staining confirmed the survival of the grafted AT (Fig. S4). The groups showed no significant difference in skin elasticity or melanin content (Fig. S5). After UVB exposure (Fig. 1d), the transplanted fat in the fat graft group remained viable (Fig. S6), and the skin

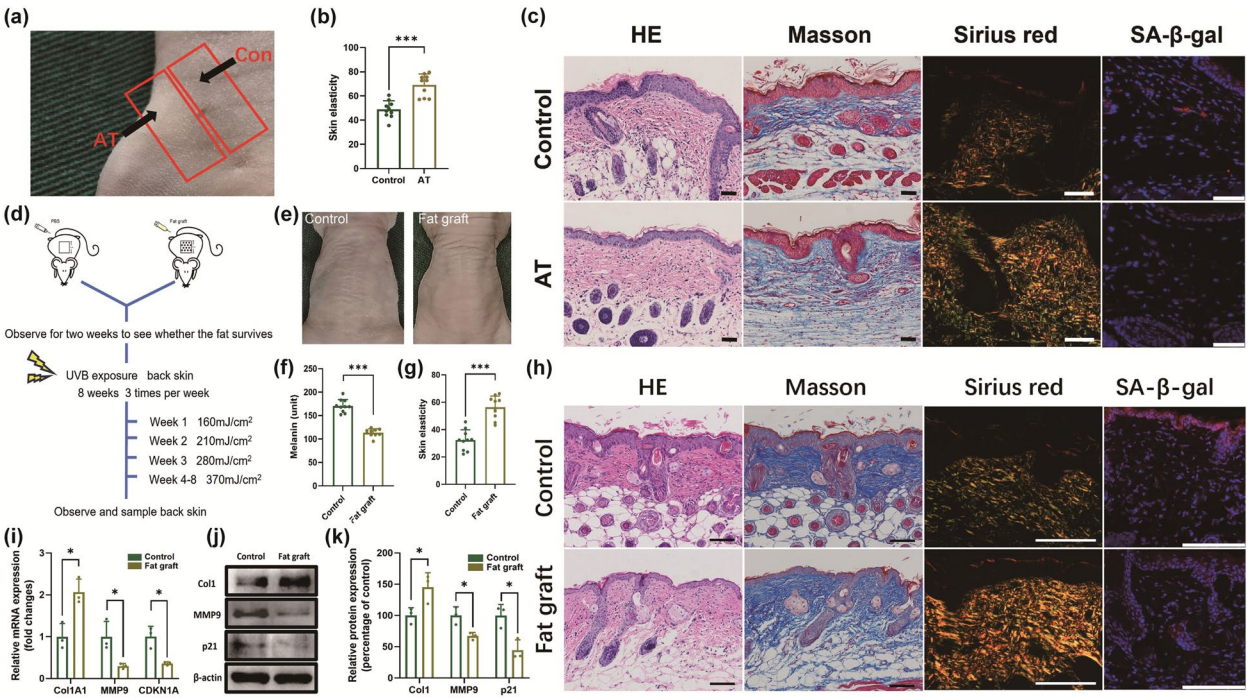

Fig. 1 AT has a protective effect on the skin under ultraviolet B (UVB) irradiation. **a** Gross image of the AT group with subcutaneous adipose tissue (SAT) in the inguinal area and the adjacent control group without SAT before UVB exposure. **b** Quantification of skin elasticity in the control group and AT group. **c** HE, Masson, Sirius Red, and immunofluorescence staining to determine epidermal thickness, dermis thickness, collagen deposition, and SA-β-gal expression in the control group and AT group. Scale bars = 50 μm. **d** Schematic diagram of fat grafting and UVB irradiation on the back. **e** Gross images of skin texture from the control group and fat graft group after UVB irradiation. **f**, **g** Quantification of the melanin content and skin elasticity in the control group and fat graft group. **h** HE, Masson, Sirius Red, and immunofluorescence staining to determine epidermal thickness, dermis thickness, collagen deposition, and SA-β-gal expression in the control group and fat graft group. Scale bars = 100 μm. **i** The mRNA expression of Col1A1, MMP9, and CDKN1A in the two groups. **j**, **k** The protein expression of Col1, MMP9, and p21 in the two groups. *$p < 0.05$, ***$p < 0.001$

appeared smoother with fewer wrinkles than that in the control group (Fig. 1e). The CK-MPA10 results revealed reduced melanin levels and improved elasticity in the fat graft group (Fig. 1f, g). Histological staining revealed that the fat graft group exhibited epidermal thinning, dermal thickening, increased collagen production, and reduced cellular senescence, which was consistent with the results from the inguinal skin model (Figs. 1h, S7). Molecular analysis, including qRT–PCR and WB, revealed the upregulation of Col1A1 and the downregulation of MMP9 and CDKN1A in the fat graft group (Fig. 1i–k). These findings further support the conclusion that the presence of AT substantially mitigates UVB-induced photoaging, leading to the rejuvenation of ageing skin.

The protective effect of AT-EVs on the skin under UVB irradiation is similar to that of ADSC-EVs

To investigate whether AT-EVs are the mechanism by which AT exerts its protective effects, we used nude mice, as shown in Fig. 2a. Previous research has demonstrated the skin-protective properties of ADSC-EVs under UVB exposure [20], establishing these EVs as positive controls. Cells from AT were cultured and differentiated into adipocytes and osteoblasts (Fig. S8) to confirm their identity. Both ADSC-EVs and AT-EVs were characterized via electron microscopy (Fig. 2b) and a flow NanoAnalyzer, which revealed average sizes of 61.3 ± 17.8 nm and 63.9 ± 18.0 nm, respectively (Fig. S9). Furthermore, both ADSC-EVs and AT-EVs expressed the surface markers CD9, CD63, and CD81 (Fig. S10) and were taken up by NIH3T3 cells labelled with PKH26 (Fig. S11).

After eight weeks of UVB exposure, the AT-EV-treated skin exhibited a reduced number of skin wrinkles (Fig. 2c). Additionally, skin elasticity and melanin content improved in the AT-EV group (Fig. 2d, e). Compared with those in the UVB group, histological analysis via HE, Masson, Sirius Red, SA-β-gal, and in situ dihydroethidium red fluorescence staining (Fig. 2f) revealed that the AT-EV group had a thinner epidermis, a thicker dermis, increased collagen levels, fewer senescent cells, and lower ROS levels (Fig. 2g-k). Furthermore, AT-EVs modulated skin gene expression, increasing Col1A1 expression and decreasing MMP9 and CDKN1A expression (Fig. 2l-n). The experimental results revealed no significant differences between the AT-EV group and the ADSC-EV group.

In summary, AT-EVs, which function similar to AT, mitigated the histological manifestations of photoaging, promoted collagen production and deposition, reduced ROS and MMP9 levels, and alleviated signs of ageing, providing skin protection under UVB exposure similar to that of ADSC-EVs. These results suggest that AT exerts its protective effects through AT-EVs.

AT-EVs also have a protective effect on NIH3T3 cells during UVB exposure and can more rapidly promote cell proliferation

For determination of the impact of AT-EVs on UVB-exposed fibroblasts, NIH3T3 and human fibroblasts were treated and analysed (Fig. 3a). AT-EVs increased Col1A1 levels while decreasing MMP9 and CDKN1A levels in NIH3T3 cells, as confirmed by both qRT–PCR and WB (Fig. 3b–d). Human fibroblasts treated with AT-EVs exhibited reduced senescence, as indicated by fewer SA-β-gal-positive cells (Fig. 3c, d), and decreased ROS accumulation, as measured via DCFH2-DA (Fig. 3g, h). The experimental results revealed no significant difference between the ADSC-EV group and the AT-EV group. Overall, AT-EVs protect fibroblasts by reducing ROS levels, promoting collagen synthesis, decreasing MMP expression, and alleviating cellular senescence. Furthermore, AT-EVs increased NIH3T3 cell proliferation more rapidly than ADSC-EVs did at 24 h post-UVB irradiation, suggesting that AT-EVs may be absorbed by cells more quickly than ADSC-EVs are, thereby exerting their effects more efficiently (Fig. 3i). These findings prompted further investigation into the mechanism by which AT-EVs can protect the skin from photoaging and be internalized more rapidly.

AT-EVs exhibit a rich variety of subpopulations, with many AT-EVs expressing CD151 and APN on their surface

The uptake of EVs is associated with the tetraspanins on their surface [32]. The differential expression of surface proteins on AT-EVs and ADSC-EVs may account for the more rapid absorption of AT-EVs by cells than that of ADSC-EVs. To investigate this finding, we compared the surface protein expression of AT-EVs and ADSC-EVs obtained from 10 patients (Fig. 4a), whose BMIs ranged from 19.473 to 30.071. We employed PBA analysis, which sorts EVs into subpopulations on the basis of their surface proteins [27]. Additionally, we compared the quantities of ADSC-EVs and AT-EVs. We used 10 ml of AT to extract ADSCs and another 10 ml of AT from the same patient to extract AT-EVs. ADSC-EVs were extracted directly without expanding the ADSC mixture. The quantities of EVs were determined via a Flow NanoAnalyzer. The number of AT-EVs was significantly greater than that of ADSC-EVs in the same volume of AT (Fig. 4b). Specifically, the count of AT-EVs in 10 ml of AT was approximately 6.1×10^{11}, which was approximately 200 times greater than the number of ADSC-EVs (Fig. 4c).

Patient data are provided in Supplementary Material 3. Principal component analysis revealed distinct surface protein expression profiles between ADSC-EVs and AT-EVs (Fig. 4d), with high correlations among biological replicates within each group, as shown by the Pearson

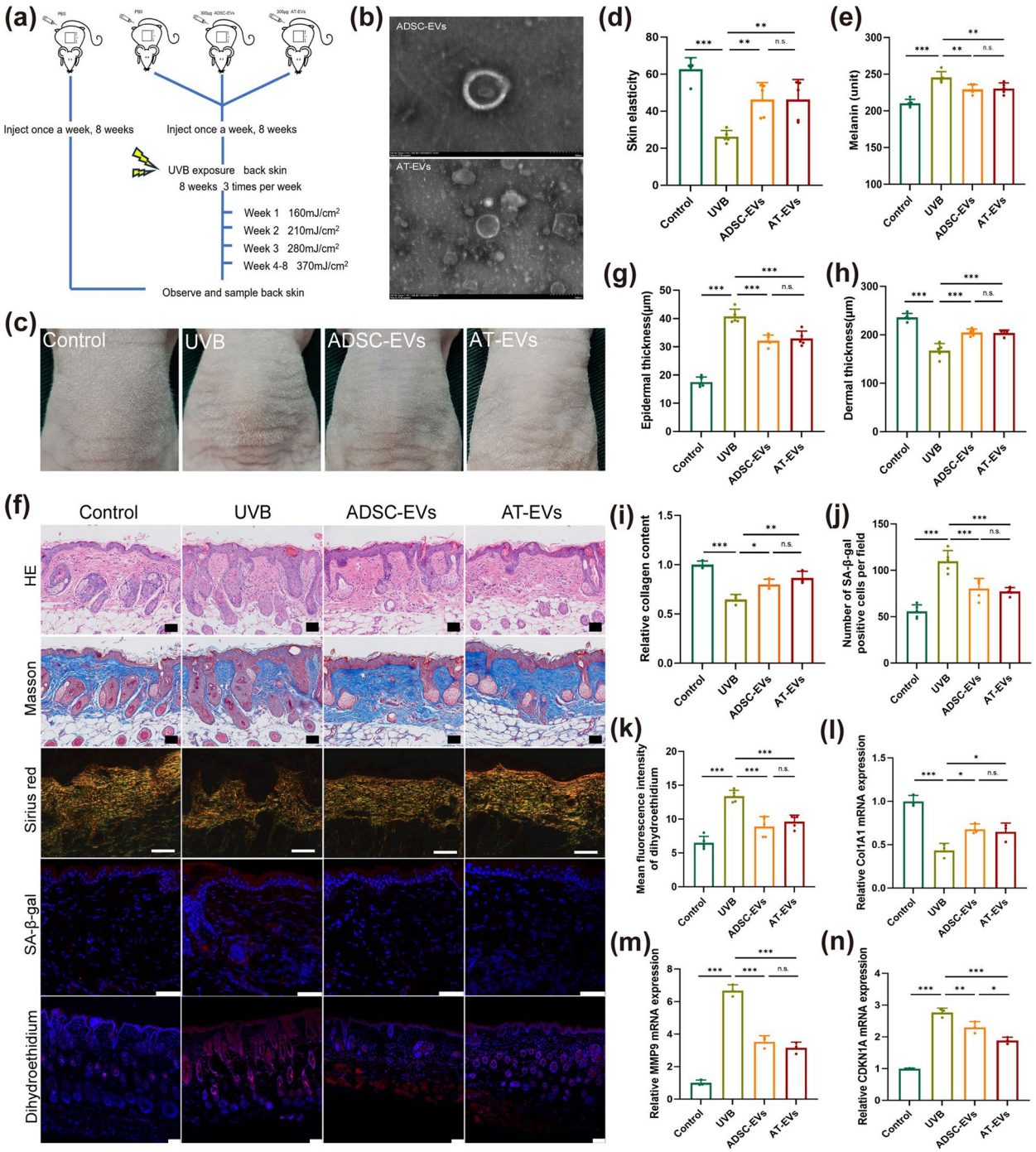

Fig. 2 AT-derived extracellular vesicles (AT-EVs) can alleviate skin photoaging caused by UVB. **a** Schematic diagram of EV injection and UVB irradiation. **b** Morphology of EVs shown by transmission electron microscopy. Scale bar = 200 nm. **c** Gross images of skin texture in the four groups after UVB irradiation. **d**, **e** Quantification of skin elasticity and melanin content in the four groups. **f** HE, Masson, Sirius Red, immunofluorescent and situ dihydroethidium red fluorescence staining to determine epidermal thickness, dermis thickness, collagen deposition, SA-β-gal expression and ROS levels in the four groups. Scale bars = 50 μm. **g**-**k** Statistical analysis of epidermal thickness, dermis thickness, collagen deposition, SA-β-gal expression, and dihydroethidium fluorescence. **l**-**n** The mRNA expression of Col1A1, MMP9, and CDKN1A in the four groups. *$p < 0.05$, **$p < 0.01$, ***$p < 0.001$, n.s., no significant difference between groups

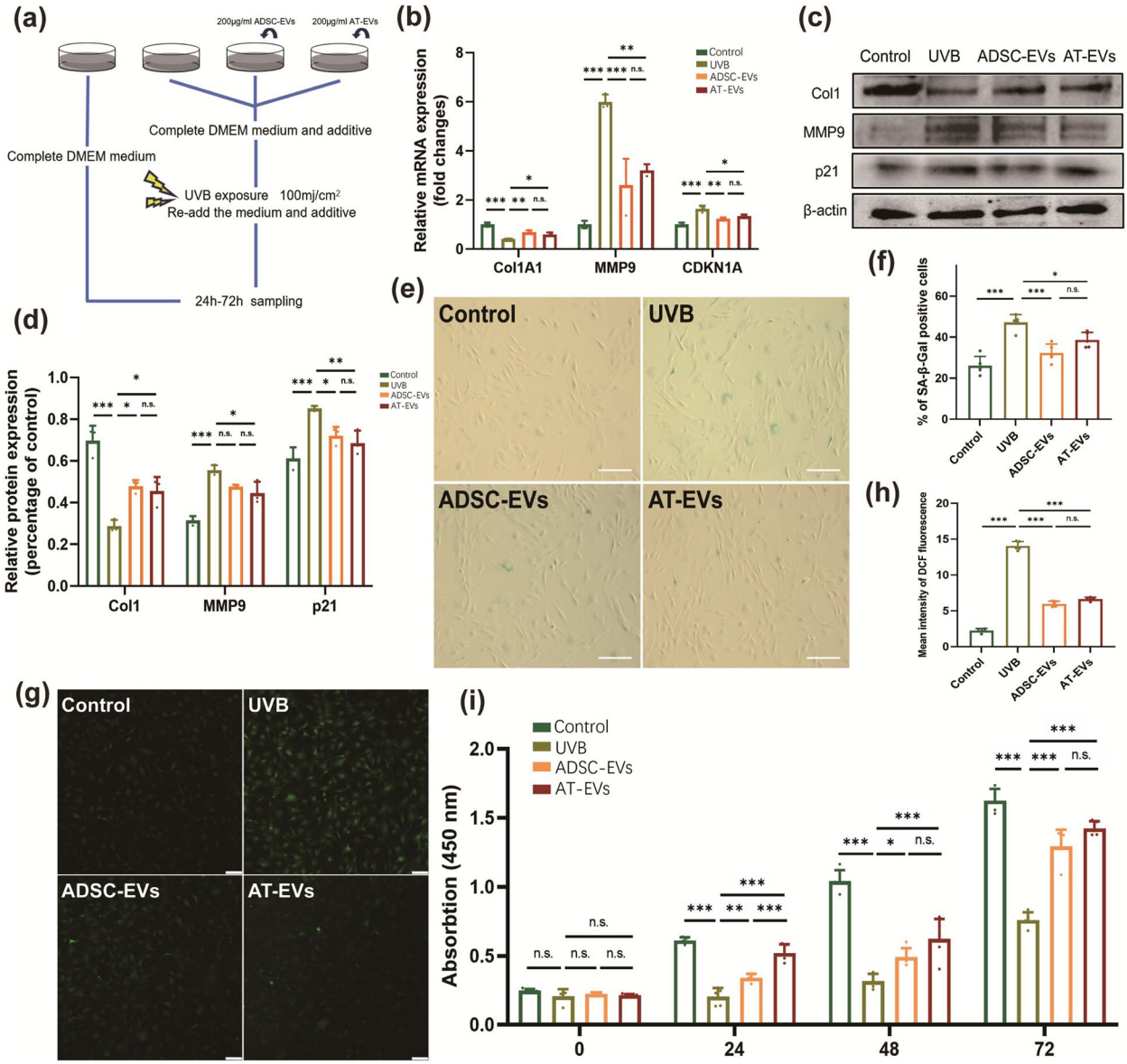

Fig. 3 AT-EVs can protect fibroblasts during UVB irradiation. **a** Schematic diagram of the process of cell intervention and UVB irradiation. **b** The mRNA expression of Col1A1, MMP9, and CDKN1A in the four groups. **c**, **d** The protein expression of Col1, MMP9, and p21 in the four groups. **e** SA-β-gal staining revealed differences in FB senescence among the four groups. Scale bars = 100 μm. **f** Quantification of SA-β-gal-positive cells in the four groups. **g** The fluorescence intensity reflects the level of intracellular ROS production after intervention and UVB irradiation. Scale bars = 50 μm. **h** Quantification of the level of ROS production in the four groups. **i** CCK-8 analysis of NIH3T3 cell proliferation in the four groups after 72 h ($n = 5$). *$p < 0.05$, **$p < 0.01$, ***$p < 0.001$, n.s., no significant difference between groups

correlation coefficient (Fig. S12). After normalization via the trimmed mean of M values method, the protein expression levels were determined (Fig. S13). A heatmap highlighted the top 100 differentially expressed surface proteins, notably showing higher levels of CD151 and AdipoQ in AT-EVs (Fig. 4e). AdipoQ in AT-EVs may have anti-inflammatory and protective effects in response to UVB exposure. t-SNE plots illustrated the clustering of EVs, distinguishing 14 clusters via FlowSOM (Fig. 4f), which were colour-coded to represent their group origins and to illustrate differences among subpopulations (Fig. 4g). The biomarkers for each cluster are shown in Fig. 4h. Most clusters exhibited positive CD151 expression. ADSC-EVs were primarily represented by one subpopulation, with cluster 1 (97.2%) characterized by the expression of AIF1, TIMP2, and FN1 (Fig. 4h, i). AT-EVs

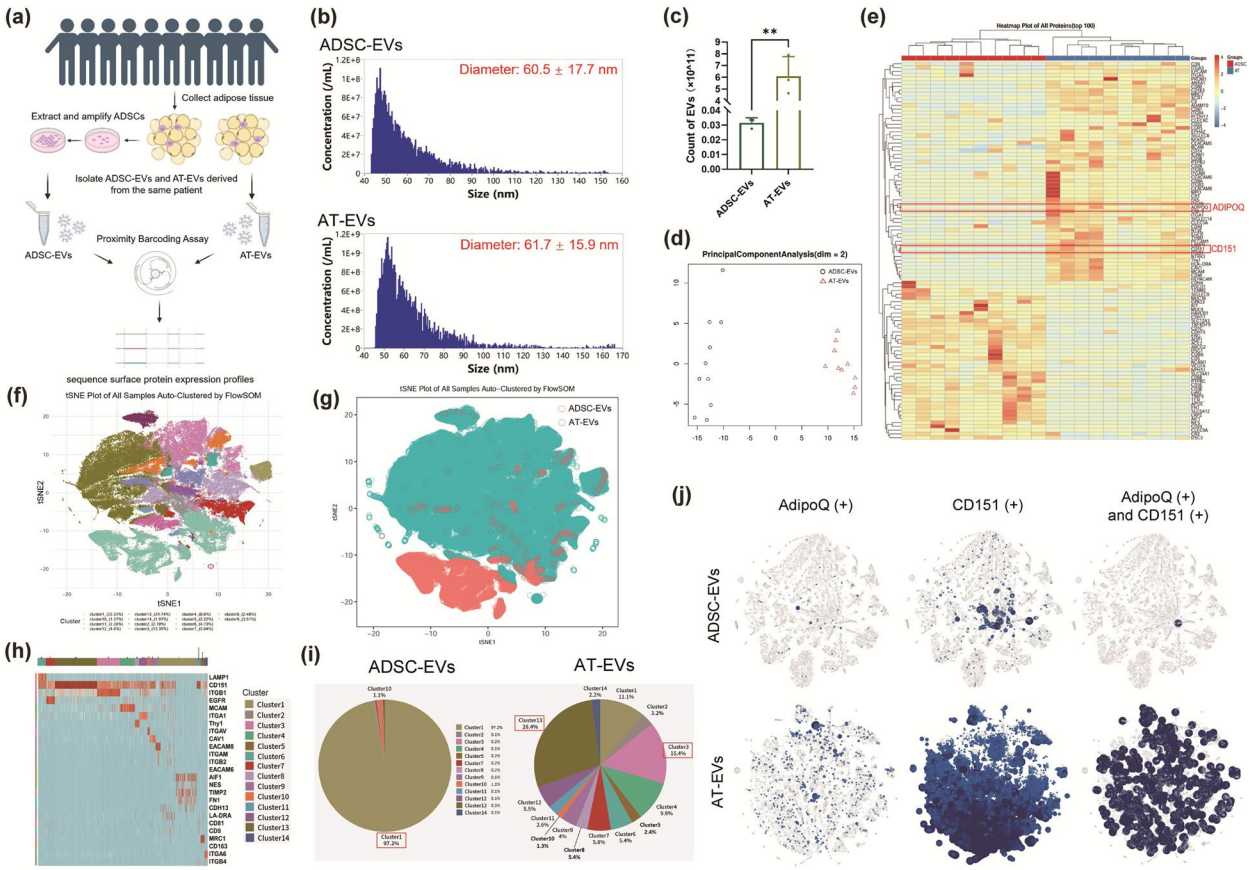

Fig. 4 Surface protein sequences and EV subpopulations of AT-EVs and ADSC-EVs. **a** Schematic diagram of sample collection and detection. **b** Flow NanoAnalyzer was used to count the number of ADSC-EVs and AT-EVs in 10 ml of AT. **c** Quantification of AT-EVs and ADSC-EVs in 10 ml of AT. **d** Principal component analysis revealed significant differences in protein expression between ADSC-EVs and AT-EVs. **e** Heatmap showing the top 100 differentially expressed proteins. **f** The FlowSOM algorithm distinguished the subpopulations of AT-EVs and ADSC-EVs, and the t-SNE plot displayed fourteen subpopulations. **g** The distribution of AT-EVs and ADSC-EVs among subpopulations. **h** Heatmap displaying the proteomic biomarker characteristics of each subpopulation. **i** Proportion of each subpopulation of ADSC-EVs and AT-EVs. **j** The expression of AdipoQ and CD151 on the surface of ADSC-EVs and AT-EVs. $^{**}p < 0.01$. (Created with BioRender.com)

displayed greater diversity and encompassed all 14 clusters. Clusters 13 and 3 had the highest proportions, at 28.4% and 15.4%, respectively. Both clusters were characterized by CD151 and ITGB1, with cluster 13 showing strong overexpression of CD151 and cluster 3 showing strong overexpression of ITGB1 (Fig. 4h, i). The analysis of surface protein expression indicated that AT-EVs had significantly higher levels of AdipoQ and CD151 than ADSC-EVs did, with 517 AT-EVs coexpressing both proteins, in contrast to only 1 ADSC-EV (Fig. 4j).

Compared with ADSC-EVs, AT-EVs presented greater surface protein diversity. We analysed surface protein expression on 13,332 EVs from both ADSC-EVs and AT-EVs. AdipoQ was expressed in 41 (0.30%) ADSC-EVs and 656 (4.92%) AT-EVs. CD151 was found in 264 (1.98%) ADSC-EVs and 11,122 (83.42%) AT-EVs. Compared with 517 (3.88%) AT-EVs, only 1 ADSC-EV showed coexpression (Fig. 4j). These findings underscore the increased subpopulation diversity, including 13 clusters beyond the primary ADSC-derived cluster, and the increased expression of key proteins such as CD151 and AdipoQ on AT-EVs, which may contribute to their increased efficacy of cellular uptake and protective effects under UVB exposure.

Adiponectin on the surface of AT-EVs activates the AMPK pathway to alleviate photoaging

We hypothesized that AT-EVs protect cells through APN during UVB exposure. To test this hypothesis, we constructed NIH3T3 cells with AdipoR knockdown (NIH3T3-shAdipoR) and treated them with ADSC-EVs and AT-EVs, with grouping and intervention, as shown in Fig. 5a. WB analysis confirmed the increased APN levels in AT-EVs (Fig. S14). We used lentiviruses to knock down AdipoR1 and AdipoR2 in NIH3T3 cells (Fig. 5b, c), and WB analysis revealed significantly reduced AdipoR

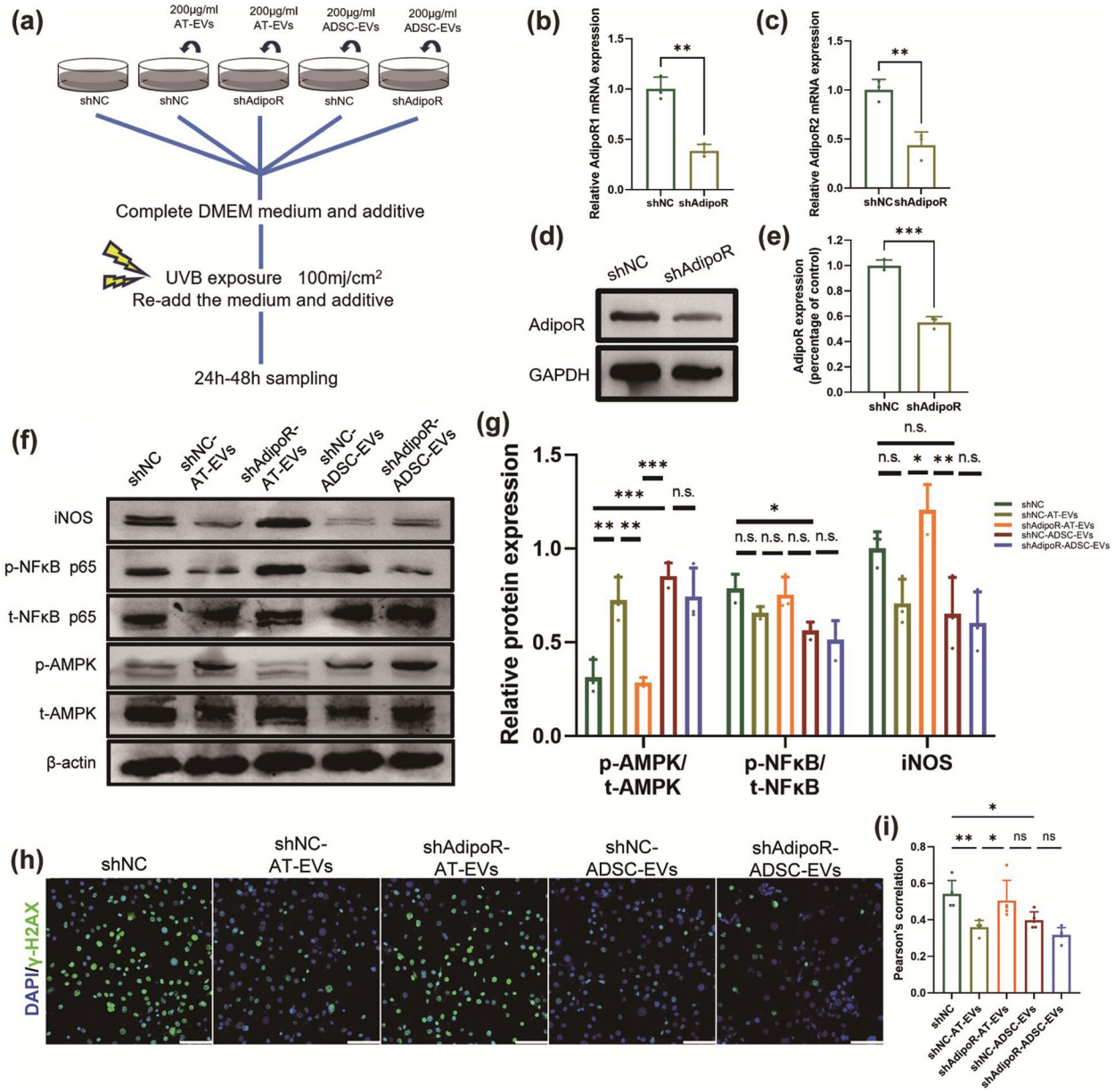

Fig. 5 APN on the surface of AT-EVs alleviates photoaging by activating the AMPK pathway in cells. **a** Schematic diagram of the intervention in each group. **b**, **c** mRNA expression of AdipoR1 and AdipoR2 in the NIH3T3-shNC group and NIH3T3-shAdipoR group. **d**, **e** The protein expression of AdipoR in the NIH3T3-shNC group and NIH3T3-shAdipoR group. **f**, **g** The protein expression of iNOS and the phosphorylation levels of AMPK and NF-κB in the five groups. **h**, **i** Immunofluorescence staining of γ-H2AX in the cell nucleus in the five groups. Scale bars = 50 μm. *$p < 0.05$, **$p < 0.01$, ***$p < 0.001$, n.s., no significant difference between groups

expression in the NIH3T3-shAdipoR group (Fig. 5d, e). WB analysis revealed a decreased ratio of phosphorylated 5′AMP-activated protein kinase^{T172} (p-AMPK^{T172}) to total AMPK (t-AMPK) in both the shNC and shAdipoR-AT-EV groups following UVB irradiation. Conversely, pretreatment with AT-EVs mitigated the UVB-induced reduction in p-AMPK^{T172} (Fig. 5f, g). We subsequently investigated the impact of AT-EVs on the activation of the NF-κB signalling pathway during UVB irradiation. Although the differences between the groups were not significant, WB analyses revealed that both AT-EVs and ADSC-EVs tended to inhibit the increase in p-NF-κB p65^{S536} levels (Fig. 5f, g). iNOS, which is downstream of the NF-κB pathway, had lower expression in the shNC-AT-EV group than in the shAdipoR-AT-EV group (Fig. 5f, g). Immunofluorescence analysis of γ-H2AX indicated

reduced nuclear DNA damage in the shNC-AT-EV group (Fig. 5h, i). These results demonstrate that APN on AT-EVs can activate AdipoR, stimulate the AMPK pathway, inhibit the NF-κB pathway, reduce UVB-induced DNA damage, and protect cells from UVB exposure.

CD151, which is highly expressed on the surface of AT-EVs, increases the cellular uptake of EVs

We investigated whether the mechanism underlying the increased uptake of AT-EVs is facilitated by the increased expression of CD151. Surface protein sequencing and WB analysis confirmed that CD151 expression was greater on AT-EVs than on ADSC-EVs (Fig. 6a). The NIH3T3 cells treated with 400 μg/ml PKH26-labelled ADSC-EVs or AT-EVs for 30 min presented increased intracellular red fluorescence in the AT-EV group (Fig. 6b, c), suggesting faster cellular uptake of AT-EVs. Moreover, the NIH3T3 cells in the AT-EV group expressed more CD151 (Fig. 6b, d). Time-lapse uptake recordings (Supplementary Material 4,5) revealed that AT-EVs were internalized earlier than ADSC-EVs were internalized, with a first appearance at 2 min 40 s for AT-EVs and 18 min 54 s for

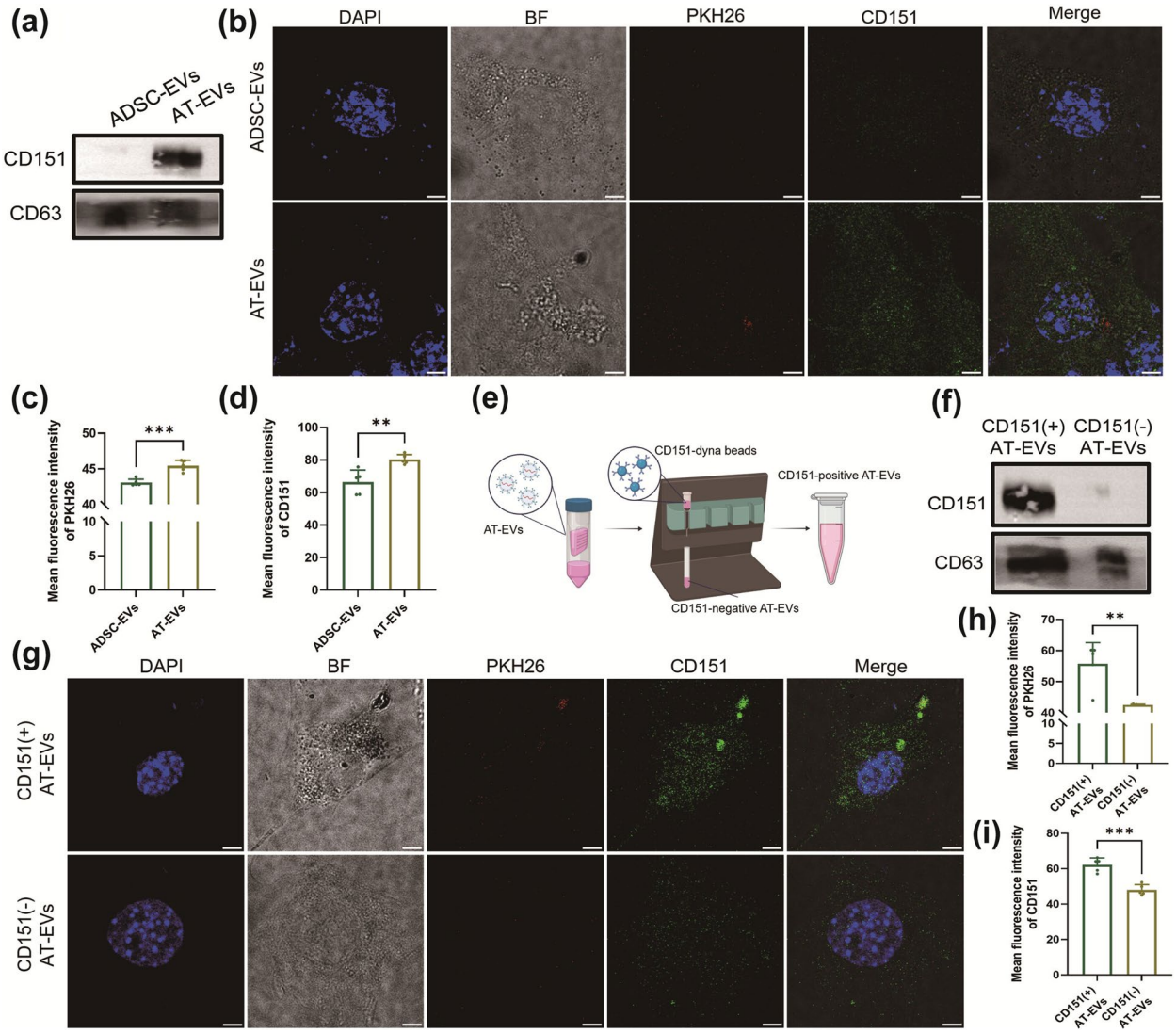

Fig. 6 AT-EVs with high expression of CD151 can be more rapidly taken up by cells. **a** The protein expression of CD151 in AT-EVs and ADSC-EVs. **b** PKH26 and immunofluorescence staining of CD151 in cells after incubation with PKH26-labelled ADSC-EVs or AT-EVs for 30 min. Scale bars = 5 μm. **c**, **d** Quantification of PKH26 and CD151 fluorescence in the AT-EV group and ADSC-EV group. **e** Sorting of CD151(+) AT-EVs and CD151(-) AT-EVs from AT-EVs. **f** CD151 expression in CD151(+) AT-EVs and CD151(-) AT-EVs. **g** PKH26 and immunofluorescence staining of CD151 in cells after incubation with PKH26-labelled CD151(+) AT-EVs and CD151(-) AT-EVs for 30 min. Scale bars = 5 μm. **h**, **i** Intracellular PKH26 and CD151 fluorescence statistics. $^{**}p < 0.01$, $^{***}p < 0.001$. (Created with BioRender.com)

ADSC-EVs (Fig. S15) and a peak fluorescence at 21 min 24 s for AT-EVs and 40 min 13 s for ADSC-EVs (Fig. S16), indicating quicker AT-EV cellular uptake and potential for earlier regulatory effects.

To investigate whether the expression of CD151 on AT-EVs facilitates faster cellular uptake than that on ADSC-EVs, we isolated CD151-positive AT-EVs from CD151-negative AT-EVs via magnetic beads (Fig. 6e). WB analysis confirmed the effectiveness of the sorting process (Fig. 6f). Both types of EVs were labelled with PKH26 and incubated with NIH3T3 cells for 30 min. Cells treated with CD151-positive AT-EVs presented increased red fluorescence, indicating faster uptake of EVs (Fig. 6g, h), as well as elevated CD151 expression (Fig. 6g, i). These findings suggest that CD151 can promote the internalization of EVs by cells.

Discussion

Photoaging, which is caused mainly by UVB, is a major external factor of skin ageing. UVB radiation triggers the MAPK/NF-κB pathway to increase MMP synthesis and suppresses the TGF-β/Smad pathway to decrease collagen expression [7]. UVB exposure also elevates the intracellular ROS level [33] and exacerbates DNA damage [34]. We utilized a dorsal skin model and a novel inguinal skin model with or without SAT to demonstrate the protective effects of SAT. Unlike artificial fat grafting, the inguinal skin with and without SAT determined the therapeutic impact of natural SAT on the skin following UVB exposure. This approach eliminates the potential complications associated with grafting errors and variations in AT survival rates. Our findings revealed that the AT group and fat graft group presented an improved skin texture compared with the control group, with a thinner epidermis, thicker dermis, more collagen, lower MMP levels, and fewer senescent cells. These results suggest that AT has a protective effect on the skin.

SAT is closely juxtaposed to the skin structurally, with notable intertissue communication. However, the mechanisms through which AT exerts regulatory effects on the skin are unclear. ADSCs in SAT can migrate to the skin, differentiate into fibroblasts, and aid in tissue repair and regeneration [35]. Vascular endothelial cells lose their adhesive ability, migrate to adjacent tissues, and differentiate into fibroblasts and myofibroblasts [16]. Nevertheless, the therapeutic effects of mesenchymal stem cells occur primarily through their paracrine actions rather than their differentiation capacity [36]. The number of ADSCs and vascular endothelial cells capable of migration and differentiation is limited. AT-EVs are crucial mediators through which AT exerts regulatory effects for paracrine and endocrine functions [19]. With respect to tissue regeneration, AT-EVs stimulate angiogenesis and collagen rearrangement during wound healing [23, 37]. Our study demonstrated that AT-EVs, similar to ATs, protect skin and fibroblasts against UVB, which potentially explains the mechanism of the protective effect of AT against photodamage.

AT-EVs, which are produced by diverse AT cells, are complex and heterogeneous vesicle mixtures [38]. Therefore, we used various technologies to isolate and study individual EVs. The mechanisms by which AT-EVs can more rapidly promote cell proliferation may be related to prompt recognition and uptake by cells, which are primarily linked to tetraspanins on the EV surface [32]. To explore the mechanism by which AT-EVs promote cell proliferation, we applied PBA sequencing, a cutting-edge and innovative technique, to evaluate surface protein expression on single particles of AT-EVs and ADSC-EVs. The PBA results revealed that AT-EVs present a variety of subpopulations, in contrast to ADSC-EVs, which have a single cluster. Among AT-EVs, 83.42% expressed CD151, and 4.92% expressed APN, whereas among ADSC-EVs, the expression rates were significantly lower, with 1.98% expressing CD151 and only 0.30% expressing APN.

The mechanism by which AT-EVs are taken up more rapidly by cells is due to the expression of CD151 on the surface of AT-EVs. CD151, a crucial transmembrane scaffold protein, interacts with integrins (ITGs), such as ITGα6β1, α6β4, α3β1, and α7β1 [39]. The ITGA6-ITGB1-CD151 complex on exosomes is linked to cancer cell invasion and metastasis [40, 41]. EVs with high CD151, ITGA6, ITGB4, and epidermal growth factor receptor vIII levels on their surface are also rapidly absorbed by recipient cells [42]. Our study revealed that AT-EVs were internalized faster than ADSC-EVs were. We innovatively separated AT-EVs via magnetic beads into CD151-positive and CD151-negative groups, with the former being more rapidly internalized. CD151 is also expressed by the cells themselves [43], so the treatment of NIH3T3 cells with CD151-negative AT-EVs also affects the expression of CD151. CD151-positive EVs have clinical application value because CD151 complexes can facilitate the rapid recognition and uptake of EVs by cells. This finding will contribute to the development of drug-loaded EVs with better therapeutic efficacy.

The protective mechanism of AT against UVB radiation is attributed to APN on the surface of AT-EVs. APN binds to AdipoR, activating the AMPK pathway, which inhibits NF-κB [44] and reduces iNOS expression, countering UVB-induced MAPK/NF-κB activation, which increases the expression of MMPs and decreases the expression of procollagen I and III [7, 45]. After AT-EV intervention, MMP9 synthesis decreases, whereas Col1A1 levels increase in fibroblasts. AMPK activation also increases mitophagy and mitochondrial biogenesis [46] to clear

damaged mitochondrial DNA [47] and reduce UVB-induced ROS [7, 8] and nuclear DNA damage [9]. Furthermore, AMPK upregulates nuclear factor E2-related factor 2 (Nrf2) for antioxidant enzyme synthesis [48, 49]. Increased mitochondrial renewal and antioxidant enzyme synthesis can eliminate the increased ROS caused by UVB. APN potentially activates the BMP/Smad pathway [50, 51], promoting cell proliferation and collagen synthesis suppressed by UVB [7, 15], suggesting a role for APN in increasing Smad pathway activity during UVB exposure. ADSC-EVs can also deliver circular RNA-Fryl to activate the AMPK pathway [52] and deliver microRNA to inhibit the NF-κB pathway [53], thereby protecting against skin photoaging.

In terms of production efficacy, AT-EVs outperform ADSC-EVs. Approximately 6.1×10^{11} AT-EVs are contained in 10 ml of AT, which is 200 times the number of ADSC-EVs in an equal volume of AT. During the standard preparation process of AT-EVs and ADSC-EVs, AT-EVs can be harvested by continuous collection in vitro within 48 h of obtaining AT. In contrast, the acquisition of a substantial amount of ADSC-EVs typically requires 2 to 3 weeks for the ADSCs to proliferate to the third or fourth generation. The acquisition of AT-EVs is significantly faster and more convenient than that of ADSC-EVs.

This study has several limitations. We focused on EV surface proteins. The cargo of AT-EVs, including microRNAs, proteins and lipids, may promote cell proliferation and migration [23] and needs further research. AT-EVs possess fourteen distinct subpopulations with varying surface proteins and potential unique functions, indicating good research value. AT-EVs, a complex mixture of molecules and diverse types of cell-derived EVs, play intricate regulatory roles in the body. Further research is needed to determine their effects on diseases such as inflammation, cardiovascular issues, and diabetes and to clinically verify their therapeutic efficacy. AT-EVs combined with APN have anti-inflammatory effects, which may also have therapeutic effects on other inflammatory diseases, such as skin fibrosis and scarring. These results will promote further studies of these diseases.

In conclusion, AT can protect skin against photodamage. The protective effects of AT are mediated through AT-EVs. The composition of AT-EVs is diverse and can be divided into 14 subpopulations. Compared with ADSC-EVs, AT-EVs have higher expression rates of CD151 and APN. The rapid internalization of AT-EVs by cells is facilitated by CD151 on the AT-EV surface. APN on the surface of AT-EVs activates the AMPK pathway, inhibits the NF-κB pathway, and reduces ROS levels in fibroblasts, thus having protective effects on UVB-irradiated cells. Furthermore, the notably greater yield and more rapid acquisition of AT-EVs than ADSC-EVs emphasize their potential clinical application.

Supplementary Information

The online version contains supplementary material available at https://doi.org/10.1186/s12964-024-01978-z.

Supplementary Material 1.
Supplementary Material 2.
Supplementary Material 3.
Supplementary Material 4.
Supplementary Material 5.

Acknowledgements
We thank BioRender for support in creating the illustrations for this publication. We are also thankful for the language polishing services provided by AJE, which have substantially contributed to the clarity and precision of our manuscript.

Authors' contributions
All the authors conceptualized the study and contributed to the methodology. Yan-Wen Wang and Poh-Ching Tan performed data curation, formal analysis, and validation. Yan-Wen Wang was responsible for visualization and wrote the original draft. Qing-Feng Li and Shuang-Bai Zhou provided funding support. Qing-Feng Li, Xue-Wen Xu, and Shuang-Bai Zhou supervised the project. All authors reviewed the manuscript.

Funding
This study was supported by grants from the National Natural Science Foundation of China (82272287), the Shanghai Clinical Research Center of Plastic and Reconstructive Surgery supported by the Science and Technology Commission of Shanghai Municipality (Grant No. 22MC1940300), the Cross-Disciplinary Research Fund of Shanghai Ninth People's Hospital, Shanghai Jiao Tong University School of Medicine (JYJC202215), the project list of the National Double First-Class and Shanghai-Top-Level high education initiatives at the Shanghai Jiao Tong University School of Medicine, and the Shanghai Key Research Center-Shanghai Research Center for Plastic Surgery (2023ZZ02023).

Data availability
The data and code underlying the findings of this study are accessible upon request to the corresponding author.

Declarations

Ethics approval and consent to participate
The study was conducted in accordance with the guidelines set by the Ethics Committee of the Shanghai Ninth People's Hospital.

Consent for publication
Not applicable.

Competing interests
The authors declare no competing interests.

Author details
[1]Department of Plastic & Reconstructive Surgery, Ninth People's Hospital, Shanghai Jiao Tong University School of Medicine, Shanghai, China. [2]Department of Plastic and Burn Surgery, West China Hospital, Sichuan University, Chengdu, China.

Received: 13 October 2024 Accepted: 3 December 2024
Published online: 18 December 2024

References

1. Martic I, Wedel S, Jansen-Dürr P, Cavinato M. A new model to investigate UVB-induced cellular senescence and pigmentation in melanocytes. Mech Ageing Dev. 2020;190:111322.
2. Ichihashi M, Ando H. The maximal cumulative solar UVB dose allowed to maintain healthy and young skin and prevent premature photoaging. Exp Dermatol. 2014;23(Suppl 1):43–6.
3. Hosseini M, Dousset L, Mahfouf W, Serrano-Sanchez M, Redonnet-Vernhet I, Mesli S, et al. Energy metabolism rewiring precedes UVB-induced primary skin tumor formation. Cell Rep. 2018;23:3621–34.
4. Lin TY, Wu PY, Hou CW, Chien TY, Chang QX, Wen KC, et al. Protective effects of sesamin against UVB-induced skin inflammation and photodamage in vitro and in vivo. Biomolecules. 2019;9:479.
5. Grether-Beck S, Wlaschek M, Krutmann J, Scharffetter-Kochanek K. Photodamage and photoaging–prevention and treatment. J Dtsch Dermatol Ges. 2005;3(Suppl 2):S19-25.
6. Cavinato M, Jansen-Dürr P. Molecular mechanisms of UVB-induced senescence of dermal fibroblasts and its relevance for photoaging of the human skin. Exp Gerontol. 2017;94:78–82.
7. Yaar M, Gilchrest BA. Photoageing: mechanism, prevention and therapy. Br J Dermatol. 2007;157:874–87.
8. Li C, Liu W, Wang F, Hayashi T, Mizuno K, Hattori S, et al. DNA damage-triggered activation of cGAS-STING pathway induces apoptosis in human keratinocyte HaCaT cells. Mol Immunol. 2021;131:180–90.
9. Jeayeng S, Wongkajornsilp A, Slominski AT, Jirawatnotai S, Sampattavanich S, Panich U. Nrf2 in keratinocytes modulates UVB-induced DNA damage and apoptosis in melanocytes through MAPK signaling. Free Radic Biol Med. 2017;108:918–28.
10. Chajchir A. Fat injection: long-term follow-Up. Aesthetic Plast Surg. 1996;20:291–6.
11. Niechajev I, Sevćuk O. Long-term results of fat transplantation: clinical and histologic studies. Plast Reconstr Surg. 1994;94:496–506.
12 Marcus BC. The use of autologous fat for facial rejuvenation. Obstet Gynecol Clin North Am. 2010;37:521–31, viii.
13. Uyulmaz S, Sanchez Macedo N, Rezaeian F, Giovanoli P, Lindenblatt N. Nanofat grafting for scar treatment and skin quality improvement. Aesthet Surg J. 2018;38:421–8.
14. Coleman SR. Structural fat grafting: more than a permanent filler. Plast Reconstr Surg. 2006;118:108s-s120.
15. Lv J, Yang S, Lv M, Lv J, Sui Y, Guo S. Protective roles of mesenchymal stem cells on skin photoaging: a narrative review. Tissue Cell. 2022;76:101746.
16. Zhang M, Chen H, Qian H, Wang C. Characterization of the skin keloid microenvironment. Cell Commun Signal. 2023;21:207.
17. Zhou SB, Zhang PQ, Zhang XJ, Tan PC, Kobayashi E, Li QF. Tracing the change and contribution of subcutaneous adipose to skin expansion using a luciferase-transgenic fat transplantation model. Plast Reconstr Surg. 2024;153:558e-e567.
18. Jeppesen DK, Zhang Q, Franklin JL, Coffey RJ. Extracellular vesicles and nanoparticles: emerging complexities. Trends Cell Biol. 2023;33:667–81.
19 Wang Y, Li Q, Zhou S, Tan P. Contents of exosomes derived from adipose tissue and their regulation on inflammation, tumors, and diabetes. Front Endocrinol. 2024;15:1374715.
20. Xu P, Xin Y, Zhang Z, Zou X, Xue K, Zhang H, et al. Extracellular vesicles from adipose-derived stem cells ameliorate ultraviolet B-induced skin photoaging by attenuating reactive oxygen species production and inflammation. Stem Cell Res Ther. 2020;11:264.
21. Zheng Y, Xu P, Pan C, Wang Y, Liu Z, Chen Y, et al. Production and biological effects of extracellular vesicles from adipose-derived stem cells were markedly increased by low-intensity ultrasound stimulation for promoting diabetic wound healing. Stem Cell Rev Rep. 2023;19:784–806.
22. Wang Y, Cheng L, Zhao H, Li Z, Chen J, Cen Y, et al. The therapeutic role of ADSC-EVs in skin regeneration. Front Med (Lausanne). 2022;9:858824.
23. Pan C, Xu P, Zheng Y, Wang Y, Chen C, Fu S, et al. Preparation of therapy-grade extracellular vesicles from adipose tissue to promote diabetic wound healing. Front Bioeng Biotechnol. 2023;11:1129187.
24. Zhang PQ, Tan PC, Gao YM, Zhang XJ, Xie Y, Zheng DN, et al. The effect of glycerol as a cryoprotective agent in the cryopreservation of adipose tissue. Stem Cell Res Ther. 2022;13:152.
25. Xu P, Yu Q, Huang H, Zhang WJ, Li W. Nanofat Increases Dermis Thickness and Neovascularization in Photoaged Nude Mouse Skin. Aesthetic Plast Surg. 2018;42:343–51.
26. Pontiggia L, Biedermann T, Meuli M, Widmer D, Böttcher-Haberzeth S, Schiestl C, et al. Markers to evaluate the quality and self-renewing potential of engineered human skin substitutes in vitro and after transplantation. J Invest Dermatol. 2009;129:480–90.
27. Wu D, Yan J, Shen X, Sun Y, Thulin M, Cai Y, et al. Profiling surface proteins on individual exosomes using a proximity barcoding assay. Nat Commun. 2019;10:3854.
28. Van Gassen S, Callebaut B, Van Helden MJ, Lambrecht BN, Demeester P, Dhaene T, et al. FlowSOM: Using self-organizing maps for visualization and interpretation of cytometry data. Cytometry A. 2015;87:636–45.
29. Cieslak MC, Castelfranco AM, Roncalli V, Lenz PH, Hartline DK. t-Distributed Stochastic Neighbor Embedding (t-SNE): A tool for eco-physiological transcriptomic analysis. Mar Genomics. 2020;51:100723.
30. Guda PR, Sharma A, Anthony AJ, ElMasry MS, Couse AD, Ghatak PD, et al. Nanoscopic and functional characterization of keratinocyte-originating exosomes in the wound fluid of non-diabetic and diabetic chronic wound patients. Nano Today. 2023;52:101954.
31. Gilhar A, Etzioni A. The nude mouse model for the study of human skin disorders. Dermatology. 1994;189:5–8.
32. Ou YH, Liang J, Czarny B, Wacker MG, Yu V, Wang JW, et al. Extracellular Vesicle (EV) biohybrid systems for cancer therapy: Recent advances and future perspectives. Semin Cancer Biol. 2021;74:45–61.
33. Thapa Magar TB, Mallik SK, Gurung P, Lim J, Kim YT, Shrestha R, et al. Chlorin E6-curcumin-mediated photodynamic therapy promotes an anti-photoaging effect in UVB-irradiated fibroblasts. Int J Mol Sci. 2023;24:13468.
34 Kim DJ, Iwasaki A, Chien AL, Kang S. UVB-mediated DNA damage induces matrix metalloproteinases to promote photoaging in an AhR- and SP1-dependent manner. JCI Insight. 2022;7:e156344.
35. Mazini L, Rochette L, Admou B, Amal S, Malka G. Hopes and Limits of Adipose-Derived Stem Cells (ADSCs) and Mesenchymal Stem Cells (MSCs) in wound healing. Int J Mol Sci. 2020;21:1306.
36. Xing X, Li Z, Yang X, Li M, Liu C, Pang Y, et al. Adipose-derived mesenchymal stem cells-derived exosome-mediated microRNA-342-5p protects endothelial cells against atherosclerosis. Aging (Albany NY). 2020;12:3880–98.
37. Cai Y, Li J, Jia C, He Y, Deng C. Therapeutic applications of adipose cell-free derivatives: a review. Stem Cell Res Ther. 2020;11:312.
38. Huang Z, Xu A. Adipose extracellular vesicles in intercellular and inter-organ crosstalk in metabolic health and diseases. Front Immunol. 2021;12:608680.
39. Sterk LM, Geuijen CA, van den Berg JG, Claessen N, Weening JJ, Sonnenberg A. Association of the tetraspanin CD151 with the laminin-binding integrins alpha3beta1, alpha6beta1, alpha6beta4 and alpha7beta1 in cells in culture and in vivo. J Cell Sci. 2002;115:1161–73.
40. Hoshino A, Costa-Silva B, Shen TL, Rodrigues G, Hashimoto A, Tesic Mark M, et al. Tumour exosome integrins determine organotropic metastasis. Nature. 2015;527:329–35.
41. Marni R, Malla M, Chakraborty A, Malla R. Proteomic profiling and ROC analysis identify CD151 and ELAVL1 as potential therapy response markers for the antiviral drug in resistant TNBC. Life Sci. 2023;320:121534.
42. Choi D, Montermini L, Kim DK, Meehan B, Roth FP, Rak J. The Impact of Oncogenic EGFRvIII on the Proteome of Extracellular Vesicles Released from Glioblastoma Cells. Mol Cell Proteomics. 2018;17:1948–64.
43. Geary SM, Cowin AJ, Copeland B, Baleato RM, Miyazaki K, Ashman LK. The role of the tetraspanin CD151 in primary keratinocyte and fibroblast functions: implications for wound healing. Exp Cell Res. 2008;314:2165–75.
44. Jian M, Kwan JS, Bunting M, Ng RC, Chan KH. Adiponectin suppresses amyloid-β oligomer (AβO)-induced inflammatory response of microglia via AdipoR1-AMPK-NF-κB signaling pathway. J Neuroinflammation. 2019;16:110.
45. Rosette C, Karin M. Ultraviolet light and osmotic stress: activation of the JNK cascade through multiple growth factor and cytokine receptors. Science. 1996;274:1194–7.
46. Song N, Xu H, Wu S, Luo S, Xu J, Zhao Q, et al. Synergistic activation of AMPK by AdipoR1/2 agonist and inhibitor of EDPs-EBP interaction recover NAFLD through enhancing mitochondrial function in mice. Acta Pharm Sin B. 2023;13:542–58.
47. Drake JC, Wilson RJ, Laker RC, Guan Y, Spaulding HR, Nichenko AS, et al. Mitochondria-localized AMPK responds to local energetics and

contributes to exercise and energetic stress-induced mitophagy. Proc Natl Acad Sci U S A. 2021;118:e2025932118.
48. Kim M, Park YG, Lee HJ, Lim SJ, Nho CW. Youngiasides A and C Isolated from Youngia denticulatum Inhibit UVB-Induced MMP Expression and Promote Type I Procollagen Production via Repression of MAPK/AP-1/NF-κB and Activation of AMPK/Nrf2 in HaCaT Cells and Human Dermal Fibroblasts. J Agric Food Chem. 2015;63:5428–38.
49 Han SH, Ballinger E, Choung SY, Kwon JY. Anti-photoaging effect of hydrolysates from pacific whiting skin via MAPK/AP-1, NF-κB, TGF-β/Smad, and Nrf-2/HO-1 signaling pathway in UVB-induced human dermal fibroblasts. Mar Drugs. 2022;20:308.
50. Meng K, Cai H, Cai S, Hong Y, Zhang X. Adiponectin modified BMSCs alleviate heart fibrosis via inhibition TGF-beta1/Smad in diabetic rats. Front Cell Dev Biol. 2021;9:644160.
51. Luo L, Zheng W, Lian G, Chen H, Li L, Xu C, et al. Combination treatment of adipose-derived stem cells and adiponectin attenuates pulmonary arterial hypertension in rats by inhibiting pulmonary arterial smooth muscle cell proliferation and regulating the AMPK/BMP/Smad pathway. Int J Mol Med. 2018;41:51–60.
52. Shen W, Zhao X, Li S. Exosomes derived from ADSCs attenuate sepsis-induced lung injury by delivery of Circ-Fryl and regulation of the miR-490-3p/SIRT3 pathway. Inflammation. 2022;45:331–42.
53. Gao W, Yuan LM, Zhang Y, Huang FZ, Gao F, Li J, et al. miR-1246-overexpressing exosomes suppress UVB-induced photoaging via regulation of TGF-β/Smad and attenuation of MAPK/AP-1 pathway. Photochem Photobiol Sci. 2023;22:135–46.

Publisher's Note

Springer Nature remains neutral with regard to jurisdictional claims in published maps and institutional affiliations.